Mechanism underlying conformational effects of the disease-associated Val66Met substitution on the intrinsically disordered region of proBDNF[†]

Ruchi Lohia,[‡] Reza Salari,[‡] and Grace Brannigan[*,‡,¶]

‡*Center for Computational and Integrative Biology, Rutgers University, Camden, NJ, USA*

¶ *Department of Physics, Rutgers University, Camden, NJ, USA*

E-mail: grace.brannigan@rutgers.edu(GB)

Selection of force field

In order to get accurate structural characterization of proBDNF with MD, we ran 500ns of T-REMD simulations of 30 residue fragment of V66 proBDNF with several commonly used ff and water model combinations. First 200ns of data was discarded as equilibration Fig S1a compares the CA shifts for Amber99sb*-ildn-q [1,2] with Tip4p-D ,[3] Amber99sbws [1,4] Amberff03sbws ,[4,5] Amber99sb-ildn with Tip3P [6] and NMR. Amber99sb-ildn with Tip4p-D and Amber99sbws gives good agreement with NMR CA chemical shift. We also compared Rg distribution for the tested ff (Fig S1b). Tip3P generates very collapsed ensembles and the remaining three ff generates similar Rg distribution. Tip3P is known to produce structures which are too collapsed relative to experiment. [3,4,7] Since, the remaining three ff gives comparable Rg, we proceed with Amber99sb*-ildn-q with Tip4p-D because it gives the best match with experiments. It has also been observed that for IDP's with little or no secondary

[†]A footnote for the title

structure, Amber99sb*-ildn-q with Tip4p-D showed good agreement with experimental NMR measurements. [8]

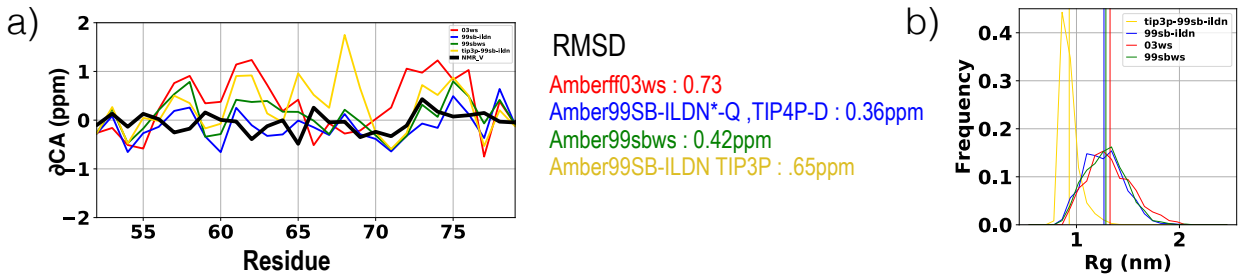

Fig S1: **Ff comparison.** (a) Comparison of calculated chemical shifts from MD ensembles at 280K and NMR chemical shifts from [9] at 280K, as described in methods. (b) Rg distribution for each ff.

Comparison with NMR

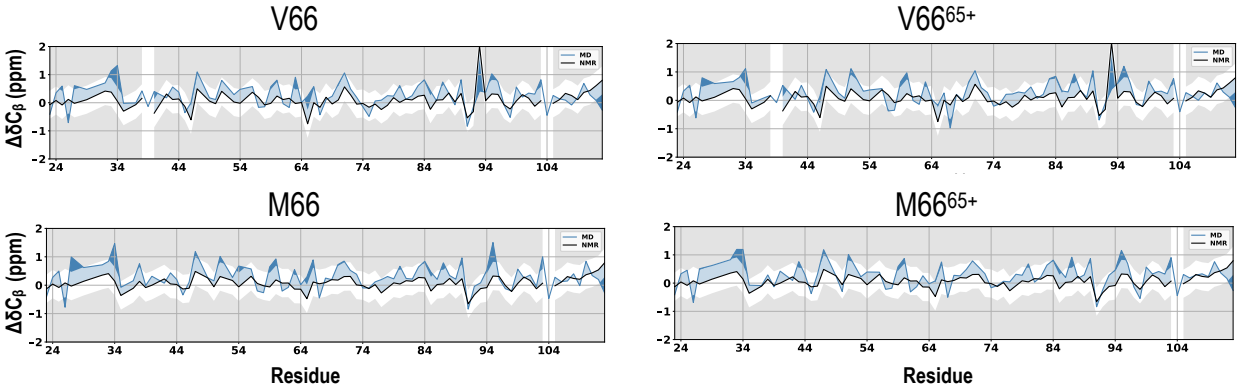

Fig S2: **Comparison of CB chemical shifts with NMR.** .

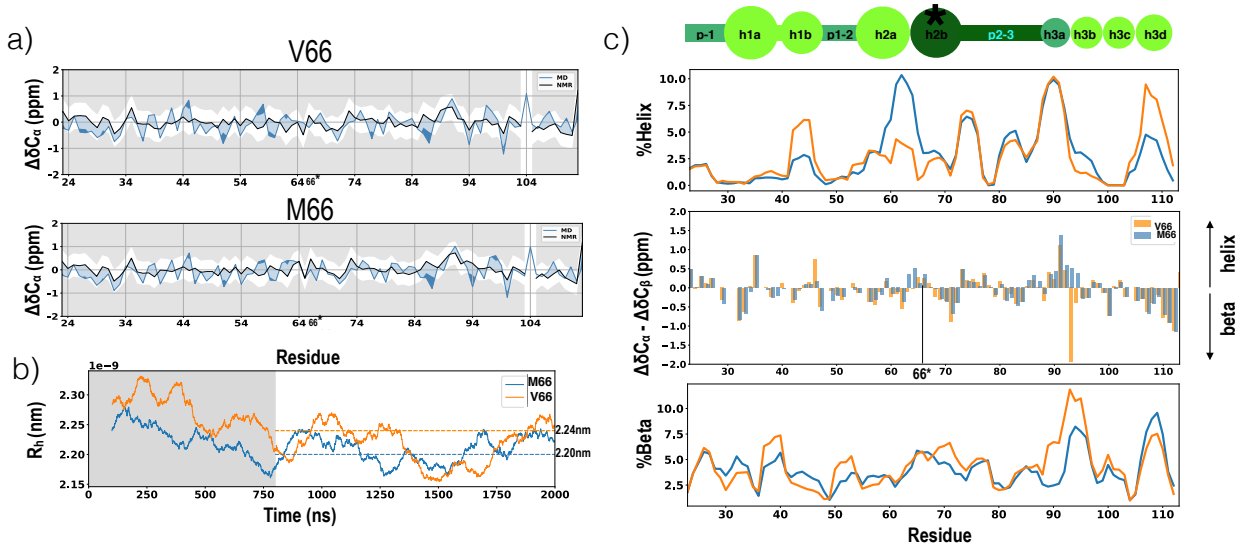

Fig S3: **Comparison of secondary structure with NMR for His65 protonated states.** .

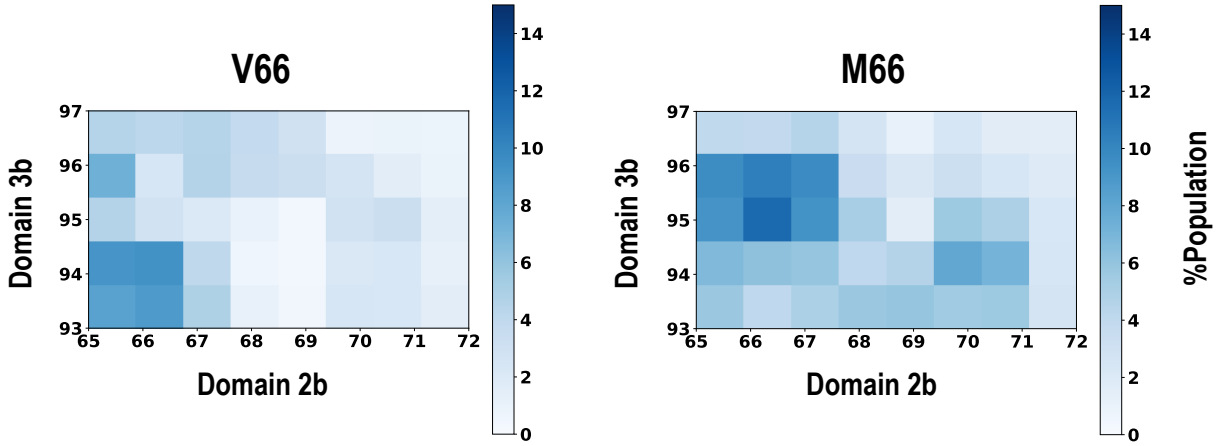

Fig S4: **Contact probablity of 2b:3b contact for V66 and M66** . .

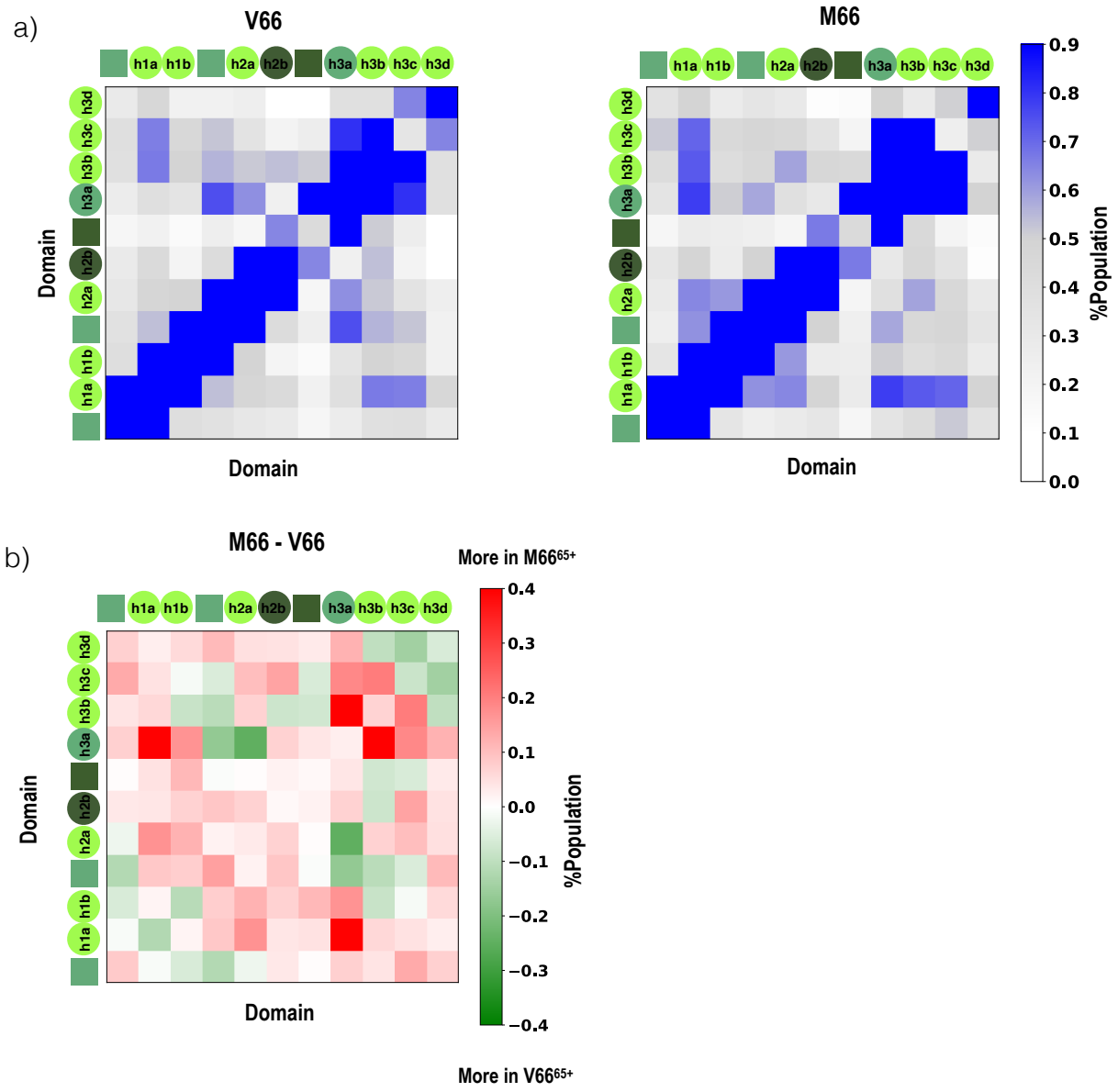

Fig S5: **Contact probability for protonated states . .**

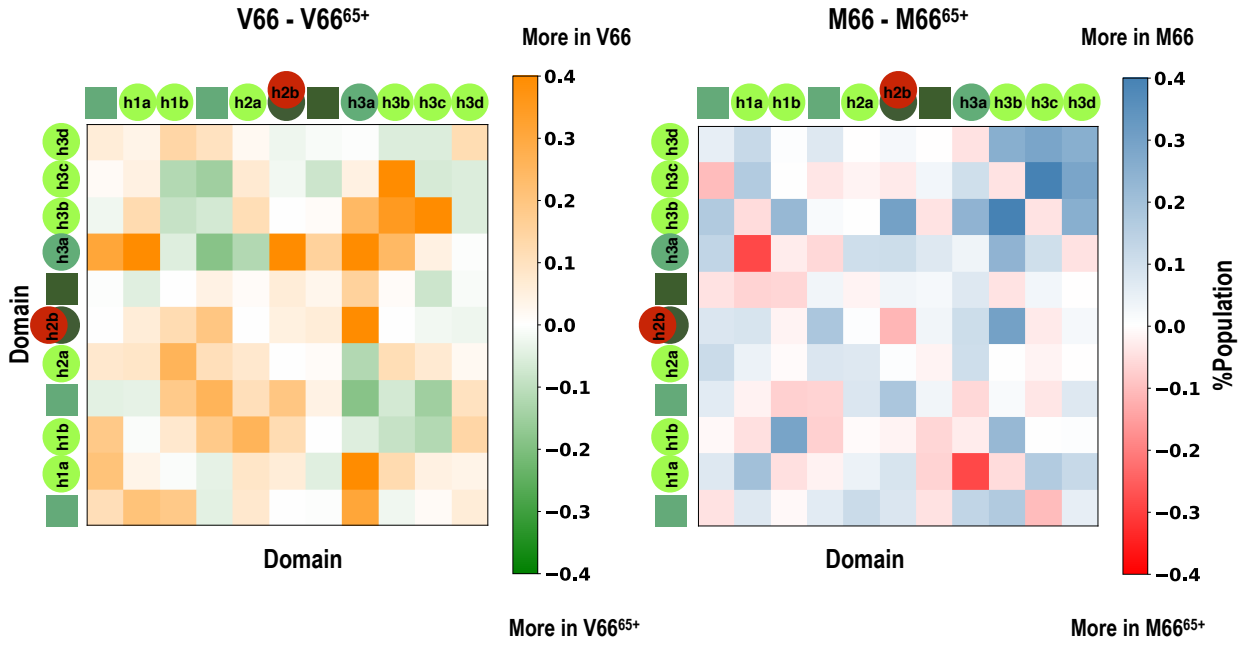

Fig S6: **Comparison of contact probability for protonated vs non-protonated states . .**

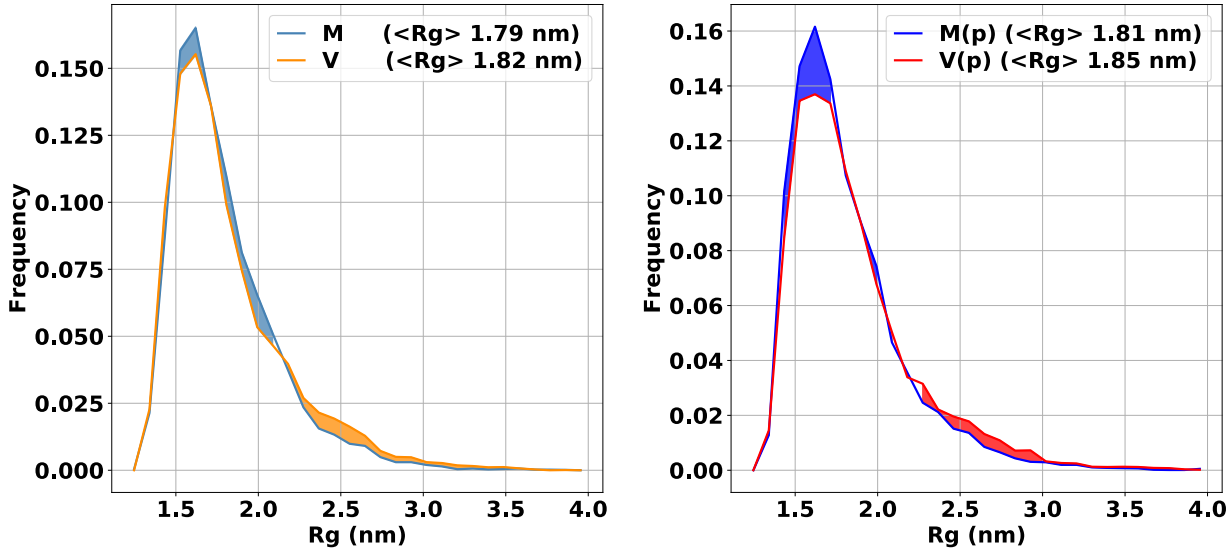

Fig S7: **Rg distribution for all four simualtions. .**

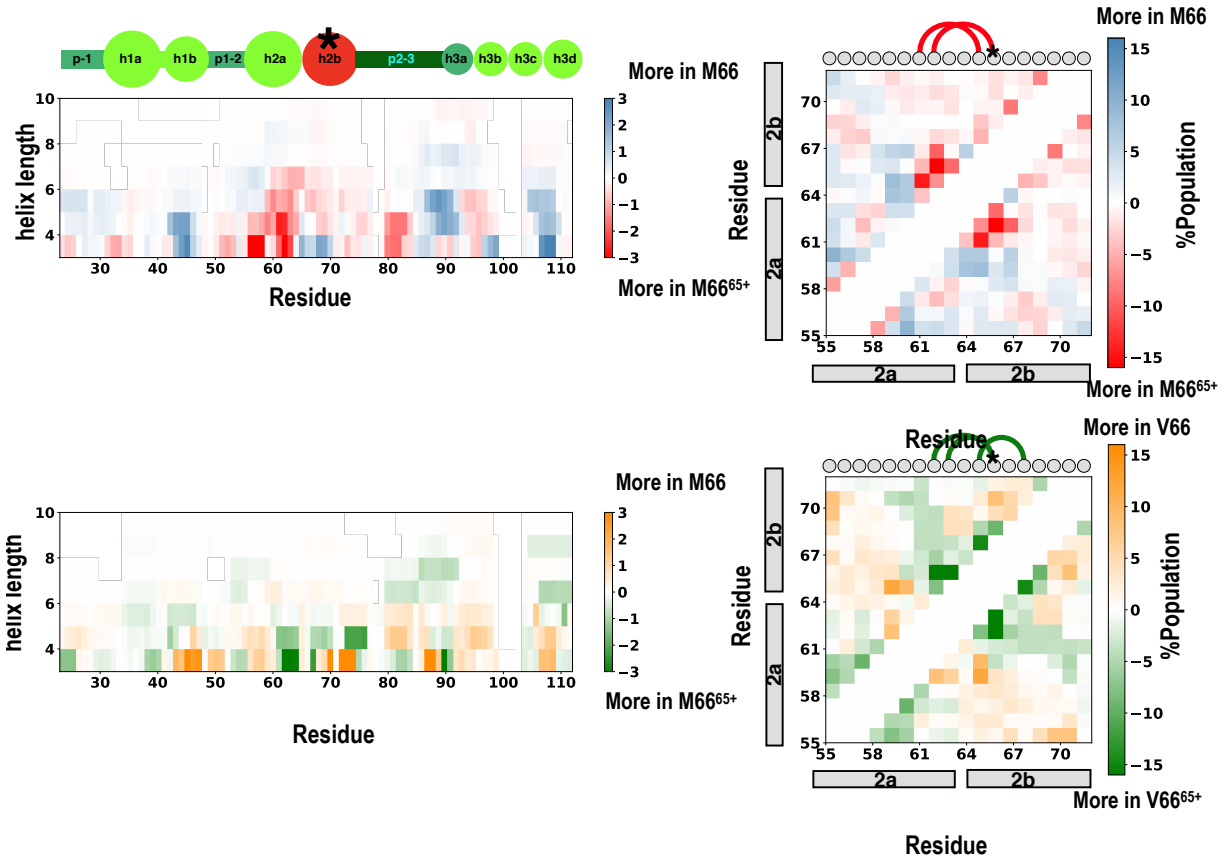

Fig S8: **Helix length and intra-domain contacts.** .

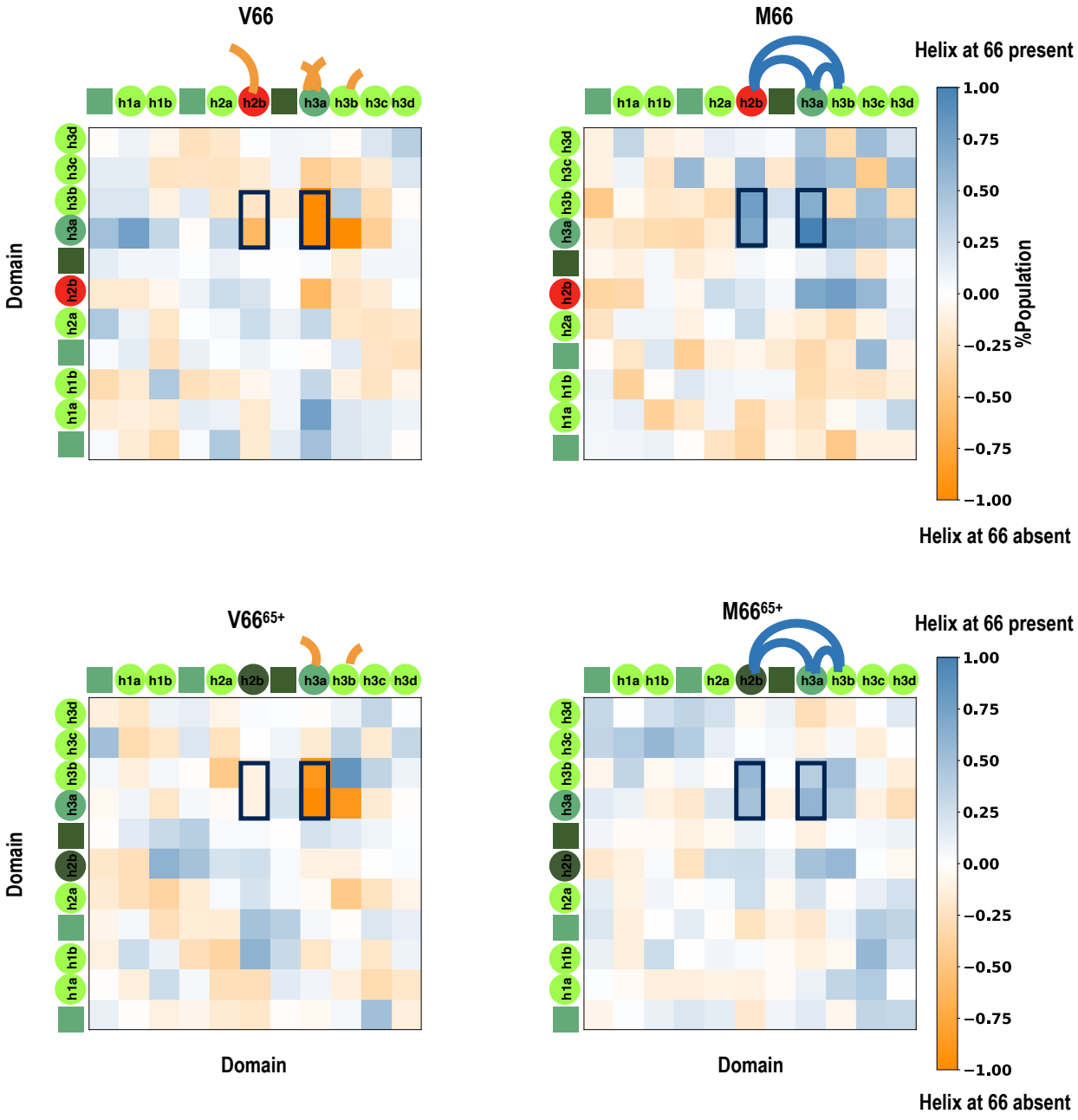

Fig S9: **Inter-domain coupling for when 66 is in helix.** .

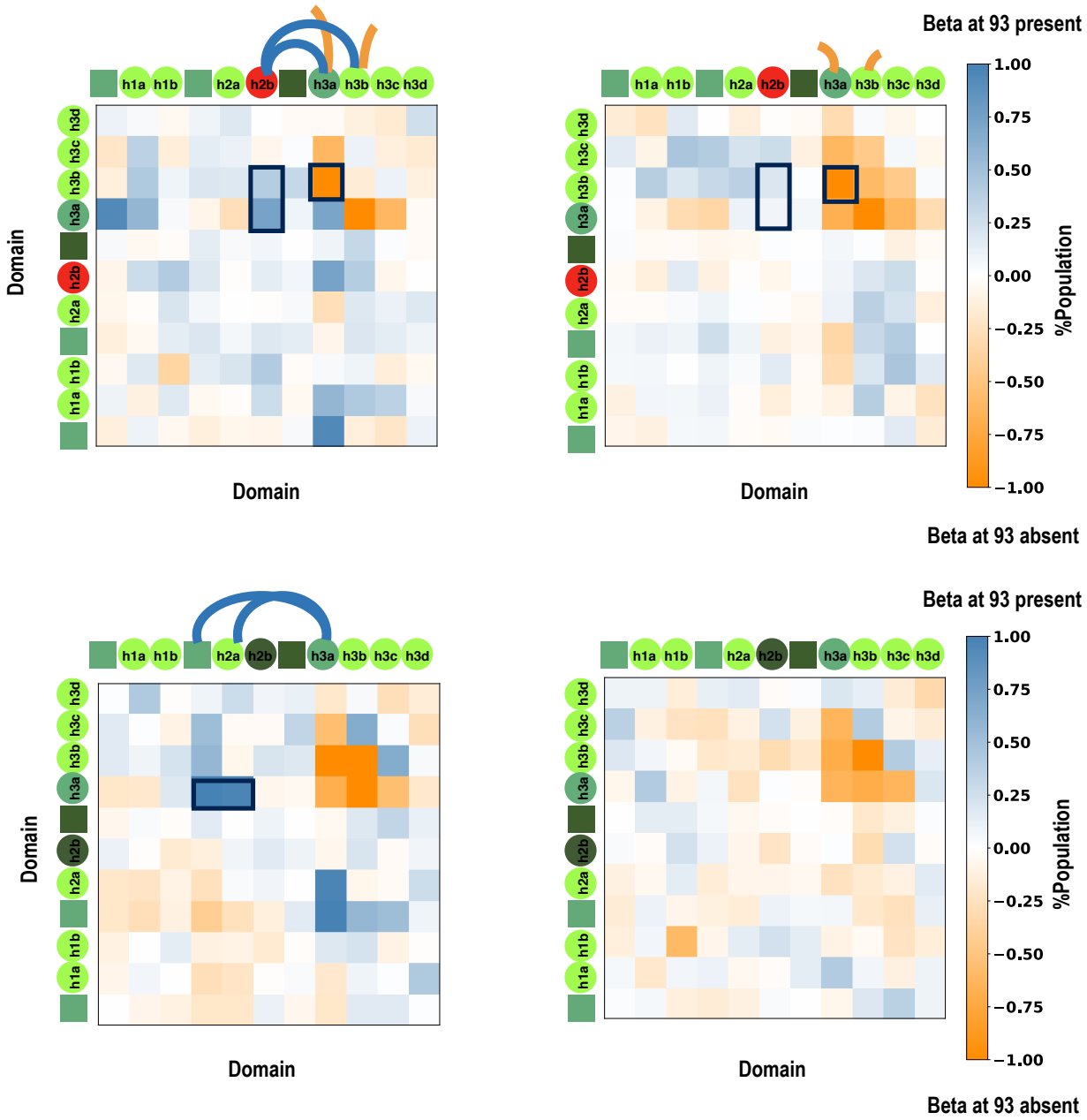

Fig S10: **Inter-domain coupling when 93 is in beta.** .

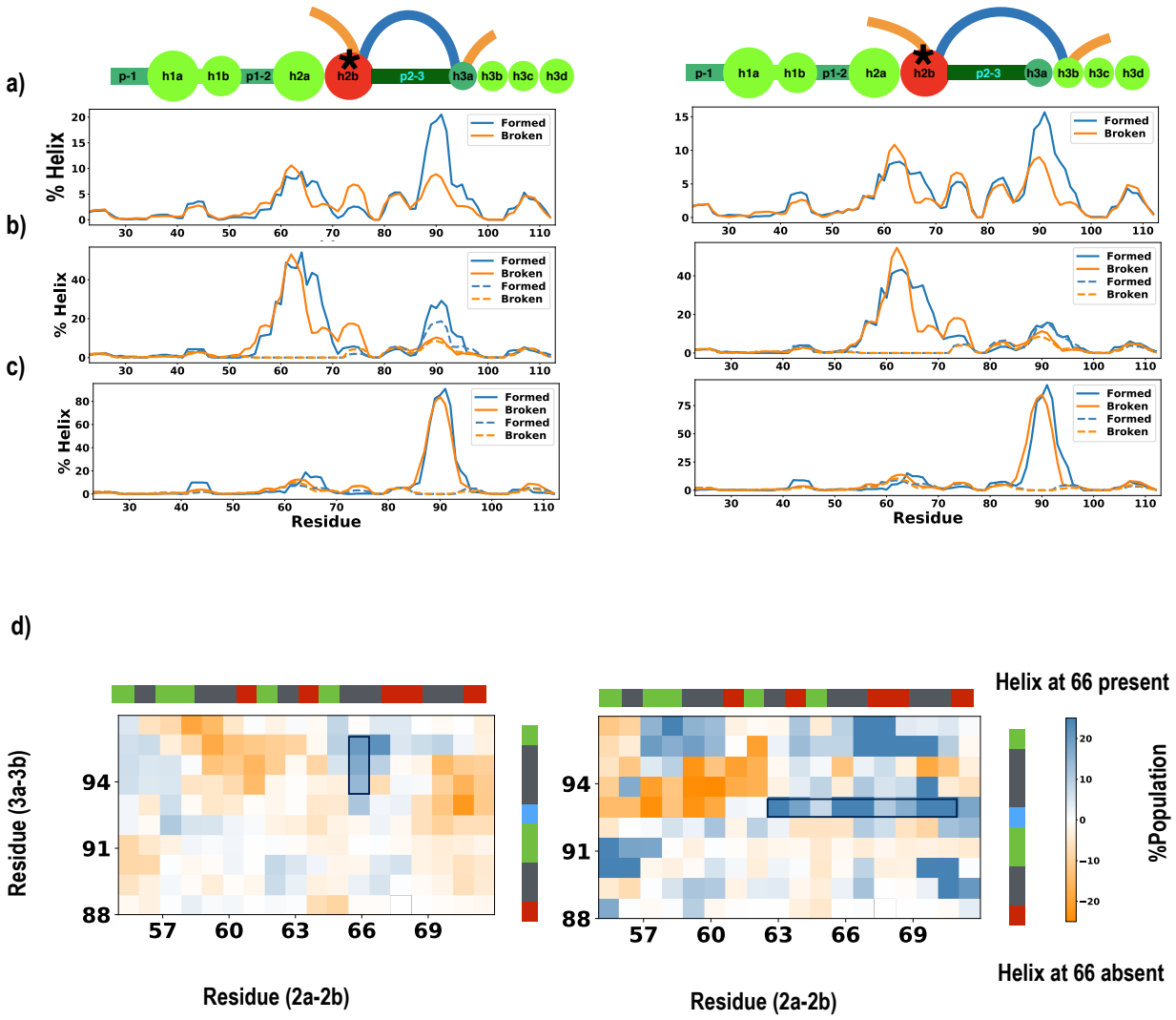

Fig S11: **Inter-domain and intra-domain coupling for M66 protonated states.** .

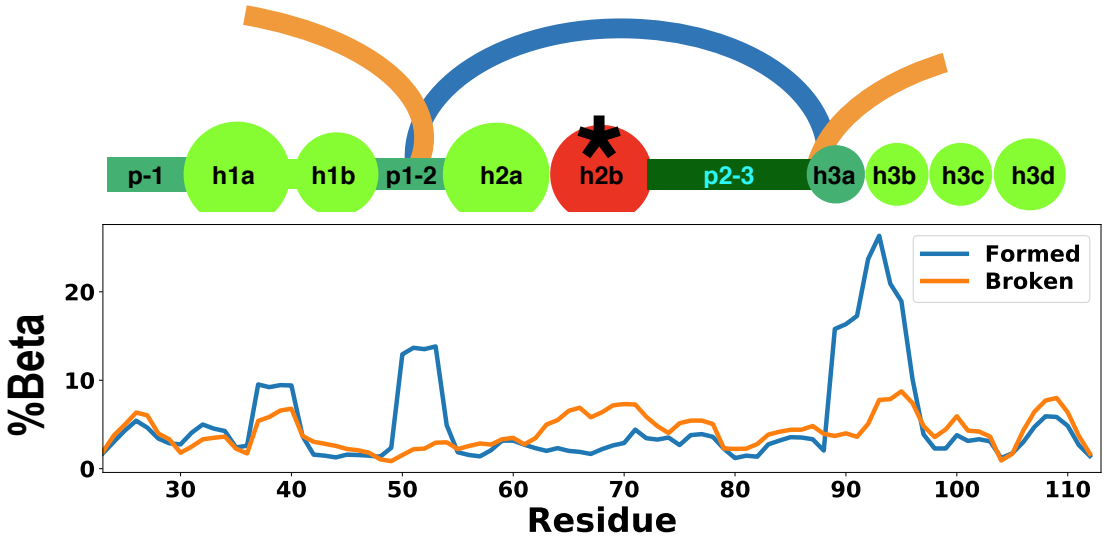

Fig S12: **Inter-domain and intra-domain coupling for V66 protonated states.** .

Simulation convergence

Most previous IDP simulations studies have been performed on smaller IDP fragments (residues 3-42) [10–12] . We performed the explicit solvent replica simulations of 91 residues, which was computationally challenging and thus we carefully accessed the convergence of our simulations. All replicas were able to diffuse in the temperature range 300K to 385K (replica round trip number >7) (Fig S13b). The Rg for V66 and M66 converge after 800ns of simulation at 300K (Fig S1b). We discarded the first 800 ns of the trajectories as conformational equilibration.

Although there are some localized discrepancies for certain residue types (Y34,L59,M95,Y113), the discrepancy is conserved across all four simulations (FigS2). Thus, these specific discrepancies are probably reflecting residual force-field inaccuracies, including the cation-pi interactions that are poorly captured by non-polarizable force felid.

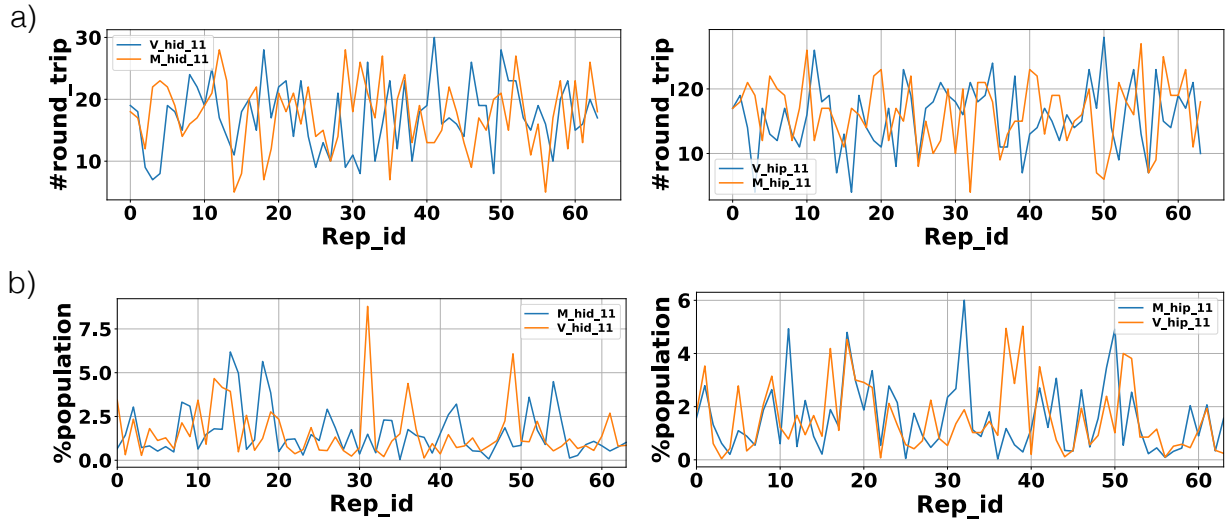

Fig S13: **Mixing of replicas during the simulation.** Time series of blocked Rg distribution and number of round trips completed by each replica for protonated His65 and neutral His65.

Tertiary contacts network

The contact networks were build using Cytoscape [?] with linear representation of residues. Each protein residue comprises a node in the network, with interactions between residues represented as edges. The strength of individual interactions can be interpreted by the thickness of the edge line on the network diagram. The transparency of an edge increases as it is found at more temperatures. If residue 66 or its neighboring residues (A51-P79) are involved in h-bond formation, its edge is drawn above the node; otherwise, the edge is drawn at the bottom of the node. To focus on significant interactions, interactions showing more than 3% persistence were considered in network visualization.

Analysis of MD Trajectories

For MD simulations, the secondary structure content was calculated with the STRIDE program incorporated in VMD,[?] which takes into account the combination of backbone dihedral angles and hydrogen bonding. Helix includes α-helix and 3_{10}-helix and β includes β-strand and β-bridge. The hydrogen bonds were calculated with |D-A|distance <= .35 nm and angle D-H-A angle <= 40?. For salt bridges, distance <= .32 nm was used as cutoff between the anionic and cationic atom. The radius of gyration was calculated using the all atoms.

References

(1) Lindorff-Larsen, K.; Piana, S.; Palmo, K.; Maragakis, P.; Klepeis, J. L.; Dror, R. O.; Shaw, D. E. *Proteins* **2010**, *78*, 1950–8.

(2) Hornak, V.; Abel, R.; Okur, A.; Strockbine, B.; Roitberg, A.; Simmerling, C. *Proteins Struct. Funct. Bioinforma.* **2006**, *65*, 712–725.

(3) Piana, S.; Donchev, A. G.; Robustelli, P.; Shaw, D. E. *J. Phys. Chem. B* **2015**, *119*, 5113–5123.

(4) Best, R. B.; Zheng, W.; Mittal, J. *J. Chem. Theory Comput.* **2014**, *10*, 5113–5124.

(5) Best, R. B.; Hummer, G. *J. Phys. Chem. B* **2009**, *113*, 9004–9015.

(6) Jorgensen, W. L. *J. Am. Chem. Soc.* **1981**, *103*, 335–340.

(7) Mercadante, D.; Milles, S.; Fuertes, G.; Svergun, D. I.; Lemke, E. A.; Gräter, F. *J. Phys. Chem. B* **2015**, *119*, 7975–7984.

(8) Robustelli, P.; Piana, S.; Shaw, D. E. *Proc. Natl. Acad. Sci.* **2018**, *115*, E4758–E4766.

(9) Anastasia, A.; Deinhardt, K.; Chao, M. V.; Will, N. E.; Irmady, K.; Lee, F. S.; Hempstead, B. L.; Bracken, C. *Nat. Commun.* **2013**, *4*, 2490.

(10) Henriques, J.; Skepö, M. *J. Chem. Theory Comput.* **2016**, *12*, 3407–3415.

(11) Rauscher, S.; Pomès, R. *Elife* **2017**, *6*.

(12) Meng, F.; Bellaiche, M. M. J.; Kim, J.-Y.; Ul, G.; Zerze, H.; Best, R. B.; Chung, H. S. **2018**,